PHOTONICS Research

Flat-field superoscillation metalens

Dingpeng Liao,[1,†] Fengliang Dong,[2,†] Kun Zhang,[1,2,†] Yi Zhou,[1] Gaofeng Liang,[1] Zhihai Zhang,[1] Zhongquan Wen,[1] Zhengguo Shang,[1] Gang Chen,[1,*] Luru Dai,[2,3] and Weiguo Chu[2,4]

[1]Key Laboratory of Optoelectronic Technology & Systems (Chongqing University), Ministry of Education, and College of Optoelectronic Engineering, Chongqing University, Chongqing 400044, China
[2]National Center for Nanoscience and Technology, Beijing 100190, China
[3]e-mail: dai@nanoctr.cn
[4]e-mail: wgchu@nanoctr.cn
*Corresponding author: gchen1@cqu.edu.cn

Received 2 May 2022; revised 29 May 2022; accepted 28 June 2022; posted 28 June 2022 (Doc. ID 462848); published 27 July 2022

Superoscillation metalenses have demonstrated promising prospects in breaking the theoretical diffraction limitations on the resolution of optical devices and systems. However, most reported superoscillation metalenses have a very small field of view of several tenths of a degree, which greatly limits their applications in imaging and microscopy. Therefore, it is of critical importance to achieve absolute high resolution by increasing the numerical apertures (NAs) of optical devices and systems. Unfortunately, similar to the case in traditional optics, it is challenging to realize a large field of view at high NA, especially in the superoscillation regime. To date, no attempt has been made to achieve flat-field focusing in the superoscillation regime, to our knowledge. Here, we demonstrate a high-NA superoscillation metalens with an entrance aperture stop, which is optimized for superoscillation performance with a comparatively large field of view. The proposed flat-field superoscillation metalens has an effective NA as large as 0.89 and achieves superoscillation focusing within a field of view of 9°. Such a superoscillation metalens may offer a promising way toward superoscillation imaging and fast-scanning label-free far-field superoscillation microscopy.

https://doi.org/10.1364/PRJ.462848

1. INTRODUCTION

Past decades have witnessed fast development and wide applications of optical super-resolution in bioscience. Fluorescent super-resolution techniques [1–3] and structured illumination microscopy [4–6] have achieved spatial resolution ranging from 100 nm down to several nanometers. However, there is an increasing demand in developing super-resolution without fluorescent labeling, which was believed forbidden by traditional optical theories. The resolution of conventional optical devices and systems is restricted to the Abbe diffraction limit of $0.5\lambda/\mathrm{NA}$ [7], where λ and NA are the working wavelength and numerical aperture, respectively. Since the concept of superoscillation was proposed [8,9], there has been growing interest in developing optical super-resolution devices for far-field operation with propagation waves [10,11]. Theoretically, an arbitrary small point-spread function can be constructed by wavefront manipulation through a properly designed superoscillation lens [12]. According to the size of the central lobe, a point-spread function can be categorized into three different types, i.e., superoscillation, super-resolution, and diffraction limited. The point-spread function is superoscillation when the spot size is smaller than $0.38\lambda/\mathrm{NA}$; it is super-resolution when the spot size is greater than $0.38\lambda/\mathrm{NA}$ but smaller than $0.61\lambda/\mathrm{NA}$; and it is diffraction limited when the spot size is greater than $0.61\lambda/\mathrm{NA}$ [13]. Label-free optical super-resolution microscopes have been demonstrated in the confocal configuration with a superoscillation lens [14] or super-resolution lens [15] as an illumination lens. Various types of superoscillatory lenses have been investigated, including linear-focusing lenses [16,17], point-focusing lenses [18–20], needle-shaped-focusing lenses [21–23], and vector wave superoscillatory lenses [24–29], for normally incident light, all of whose fields of view are limited to an order of one-tenth degree. This greatly restricts the performance of superoscillation lenses and the imaging acquisition rate of super-resolution confocal microscopes utilizing superoscillation lens illumination. Therefore, developing wide-angle superoscillation lenses or flat-field superoscillation lenses is of great importance for such applications.

Recent development in metasurfaces [30,31] has provided alternatives to realize diffractive lenses in more flexible ways through manipulation of amplitude [32], phase [33,34], polarization [35], and dispersion [36] at a sub-wavelength scale. Different approaches have been reported on realizing wide-angle metalenses. A 40°-wide-angle metalens with NA of 0.4 [37] has been demonstrated by optimizing the lens phase profile and an aperture stop; a doublet with NA of 0.44 has

achieved 50°-wide-angle performance [38]; a doublet with NA of 0.49 has also been demonstrated for a wide angle of 60° [39]; using a quadratic metalens, wide-angle operation as large as 80° and a high NA of 0.89 have been achieved [40]. However, the resolution of all reported wide-angle metalenses is restricted by the fundamental Abbe diffraction limit. Recently, a few trials have been conducted to achieve flat-field operation in the super-resolution regime. A super-resolution singlet metalens [41] has been proved effective for obliquely incident light. The lens has a radius of 240λ, focal length of 60λ, and high NA of 0.97, and its spot size remains approximately 0.45λ on the focal plane within an incident angle range of $\pm 2°$, showing little fluctuation. A 50°-wide-angle super-resolution doublet [42] has been reported with an NA of 0.45. Simulation results have shown that the spot size varies between 0.75λ and 0.78λ in x direction and between 0.772λ and 0.931λ in y direction (on the incident plane of yoz), clearly broadened in y direction. The small NA results in a spot size greater than half-wavelength. Actually, even in conventional optics, it is also challenging to increase the field of view at large NA. For a commercialized objective lens with an NA of 0.95, its field of view is approximately 10°.

To date, no attempt has been made to achieve flat-field focusing in the superoscillation regime with a comparatively large field of view. In the present work, utilizing geometric phase metasurfaces, a high-NA dielectric singlet metalens with an entrance aperture stop has been demonstrated for superoscillation focusing within a field of view of 9° at a wavelength of $\lambda = 632.8$ nm. Such a high-NA flat-field superoscillation metalens can be applied in superoscillation imaging and fast image acquisition for far-field label-free superoscillation confocal microscopy.

2. PRINCIPLE AND DESIGN

Figure 1(a) schematically illustrates the focusing by the flat-field superoscillation metalens, and Fig. 1(b) shows the a-Si cubic geometric-phase meta-atom [43,44] for wavefront manipulation of the metalens. The metalens is composed of a metasurface behaving as a superoscillation focusing lens and an optical aperture stop aiming to further reduce the off-axis aberration, which are integrated on two sides of a SiO_2 glass substrate. Considering the latter's fabrication capability, for a given pitch of $P = 270$ nm and height of $H = 436$ nm, the transverse size of the a-Si meta-atom has been optimized for reasonably high-efficiency phase modulation of cross-polarization under illumination of circularly polarized light at a wavelength of $\lambda = 632.8$ nm by using the finite-difference time-domain (FDTD) method. The complex refractive index used for optimization is $3.02 + i0.005$ for a-Si and 1.457 for SiO_2 substrate (v015.04-1107, Plan Optik AG). The refractive index of a-Si is experimentally measured by a spectroscopic ellipsometer (SE-850 DUV, SENTECH Instruments GmbH). The optimized sizes are $L_x = 186$ nm and $L_y = 88$ nm, resulting in an amplitude transmittance of 80%. By rotating the a-Si block in the xy plane by an angle of γ, the transmitted cross-polarized circularly polarized light gains a phase shift of $\phi = 2\gamma$.

Compared with a previously reported super-resolution singlet metalens [41], the present superoscillation lens is designed with the same basic parameters, i.e., lens radius and focal length. For a given thickness of the SiO_2 substrate $d = 175$ μm, radius of the focusing metalens $R_F = 240\lambda$, and focal length of $f = 60\lambda$, the phase profile $\varphi(x, y)$ and aperture stop radius R_A of the flat-field high-NA superoscillation metalens are optimized by using the particle-swarm method (PSM) [45], aiming to minimize the off-axis aberration of superoscillation focusing within the target incident angle range of $\pm 4.5°$. In many practical applications, such as telescopes and microscopes, only transversely polarized fields participate in the final imaging. Therefore, in the present design, only the transverse polarization components are considered. The focused optical fields are obtained by using a two-dimensional angular spectrum method [46]. According to the diffraction patterns on the focal plane, the focusing performance parameters are obtained, including focal spot peak intensity, focal spot size, focal spot displacement, and sidelobe ratio (the intensity ratio between the maximum sidelobe and central lobe).

The optimized aperture stop has a radius of $R_A = 118\lambda$, and the phase profile $\varphi(x, y)$ is illustrated in Fig. 2(a); detailed information can be found in Table 1, which gives the phase distribution of lenses along the radial direction. In the table, the phase number is given by p_i in the base-32 numerical system for the meta-atom at the location $(i-1)P$ away from the lens center, and the phase value of φ_i is equal to $2\pi p_i/32$. Although the radius of the entire lens is $R_F = 240\lambda$, only a part of the focusing lens is illuminated due to the restriction of the aperture stop. Therefore, the effective NA of the entire lens is approximately 0.89.

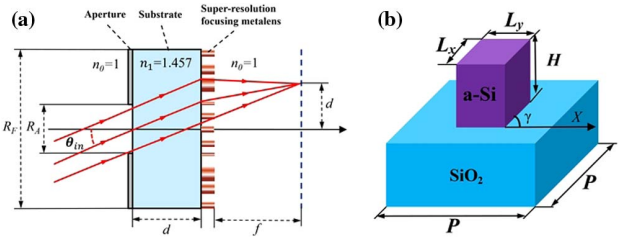

Fig. 1. Flat-field superoscillation metalens. (a) Schematic illustration of focusing of off-axis light by a flat-field superoscillation metalens. (b) Schematic illustration of the a-Si dielectric meta-atom for geometric-phase manipulation in the metalens.

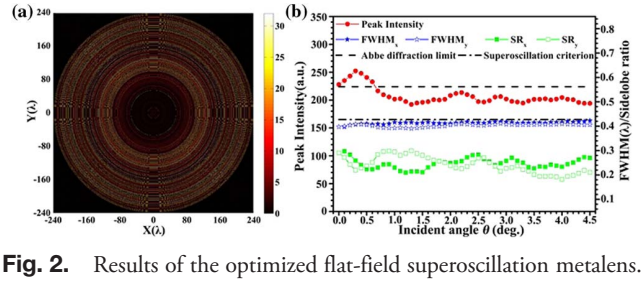

Fig. 2. Results of the optimized flat-field superoscillation metalens. (a) Phase profile of the lens $\varphi(x, y)$; (b) peak intensity (red solid), full width at half-maximum $FWHM_x$ (blue solid) and $FWHM_y$ (blue open) in x and y directions, and sidelobe ratio in x (green solid) and y (green open) directions at different incident angles.

Table 1. Phase Distribution along Radial Direction

No. of Rings	Phase of Rings (p_i) $\varphi_i = 2\pi p_i/32$
#1–#140	00C040000J5000000060000060000000D00000000 10000000000000000042000000040000000000000 00000000200020000000000000000020000000000 00000N001000063302
#141–#280	000301442010C4400010110440000444310054464 1440054454040415474570FD4001F000C88A00910 B207003005546W0CQG010QJ09H0F5XH2SG 2F7PGQBE1F2P00W64CP44M32
#281–#420	APA6A7P7B4AQG4QBQ4523VZ8EHKFN7N3322 Y562F73A22EG325250YQ3312175035E6C290RB 40S002XB10330210R6Z0D50305V2004005Y014M 171YQ03P0KAF4K60448D010A90H0
#421–#562	M0R001E4C20Q84463X20MAM20054P8A0C2E0B 070B0W0HC6WJR200N00X12M0P0F0H0GD0S4 M2C383K0H0K0BX8S1027Z5P2Z0Q2H2JAGS3Q 060M110E063MC20072200Q3G0E00N0M0D0

Figure 2(b) presents the focusing performance parameters, i.e., intensity, focal spot size, and sidelobe ratio, at different incident angles. The theoretical results of previously reported wide-angle super-oscillatory doublets [42] show a fast increase in spot size in the incident plane as the incident angle increases. However, in the present work, it is clearly seen that the intensity (red) varies between 190 and 260, and the spot size (blue) has a very small fluctuation between 0.391λ and 0.42λ, which is much smaller than the Abbe diffraction limit of 0.562λ (0.5λ/NA) and is also smaller than the superoscillation criterion of 0.427λ (0.38λ/NA) [13]. Therefore, the lens is superoscillatory. In optimization of the flat-field superoscillation metalens, we optimized only the spot size and sidelobe of the focal spot within the angular field of view, and did not put any restriction on the intensity fluctuation at different incident angles. Therefore, there exists a clear variation in intensity when the incident angle changes. Such fluctuation can be reduced by setting a restriction on intensity, but it will take more time for optimization of the lens. It is also noted that the spot size has a very small difference in x and y directions. Although the effective NA is comparatively smaller, the spot size is even smaller than the previously reported size of 0.46λ [41], which demonstrates the advantage of using the optical aperture stop in the flat-field superoscillation metalens, realizing superoscillation focusing and greatly increasing the field of view as well. The sidelobe ratio (the ratio of maximum sidelobe intensity to the peak intensity, green) remains below 30% in the entire target incident angle range. According to our simulation, the spot size is 0.436λ as the incident angle increases to 5°, but with a sharp increase in the sidelobe ratio up to 40%. Compared with the previously reported super-resolution metalens singlet for focusing of obliquely incident light, due to the optimized optical aperture stop, the field of view of the present lens has been enhanced by a factor of two. More importantly, the present lens already works in the superoscillation regime, and a field of view of 9° is comparable to commercialized diffraction-limited high-NA flat-field objective lenses.

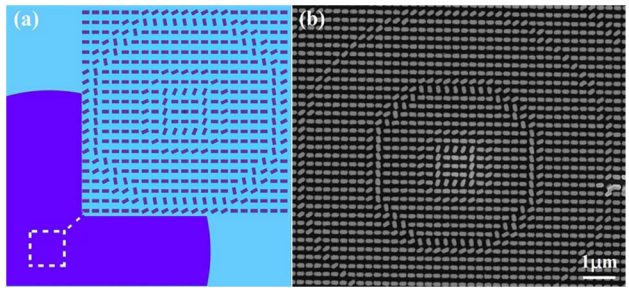

Fig. 3. (a) Diagram of the superoscillation focusing metalens arrangement in square lattice array, where inset gives the arrangement of the meta-atoms located at the device center. (b) SEM picture of the central part of the fabricated flat-field superoscillation metalens.

3. LENS FABRICATION

A 175-μm-thick SiO_2 plate is first cleaned by traditional piranha solution (a 3:1 mixture of sulfuric acid and 30% hydrogen peroxide) and acetone. A 445-nm-thick a-Si layer is deposited on the front side of the SiO_2 substrate by using inductively coupled plasma enhanced chemical vapor deposition (Sentech SI 500D, SENTECH Instruments GmbH). Then a 50-nm-thick aluminum film hard mask is grown on both sides of the device by using magnetron sputtering. A double-side mask aligner is used to make the gold alignment marks on both sides of the device. The pattern of the optical aperture stop is transferred to the hard mask using e-beam lithography (Vistec EBPG 5000plus ES, Vistec Electron Beam GmbH), and inductively coupled plasma etching (Sentech PTSA SI 500, SENTECH Instruments GmbH) is applied to form the aperture stop on the front side of the device. The metalens is fabricated with the same method. Figure 3 presents a diagram of the focusing metalens and an SEM picture of the fabricated flat-field superoscillation metalens.

4. RESULTS AND DISCUSSION

We characterized the fabricated flat-field superoscillation metalens by illuminating it with a collimated $\lambda = 632.8$ nm laser beam at different incident angles and measuring its optical intensity distribution on the designed focal plane at $z = 60\lambda$. A linearly polarized 632.8 nm He–Ne laser (HNL210L, Thorlabs, Inc.) is used as the coherent light source; a linear polarizer is used as an intensity filter to control the illumination power on the metalens; the beam size is enlarged by a beam expander (BE02-05-A, Thorlabs, Inc.); the expanded beam is sent to mirror #2 mounted on a rotation stage with a rotation angle resolution of 5 arcmin (PR01/M, Thorlabs, Inc.); then the beam is reflected and impinged on the back side of the metalens. The diffraction pattern of the metalens is then captured by a high-NA-optical-microscope-based testing system, composed of an infinite objective lens (CF Plan 100 × /0.95, Nikon), a one-dimensional nanopositioner (EO-S1047, Edmund Optics), a tube lens (ITL200, Thorlabs, Inc.), and a high-resolution digital camera (acA3800-14 μm, Basler, Inc.). The incident angle can be precisely controlled by fine rotating the rotation stage. The images of the diffraction pattern on the

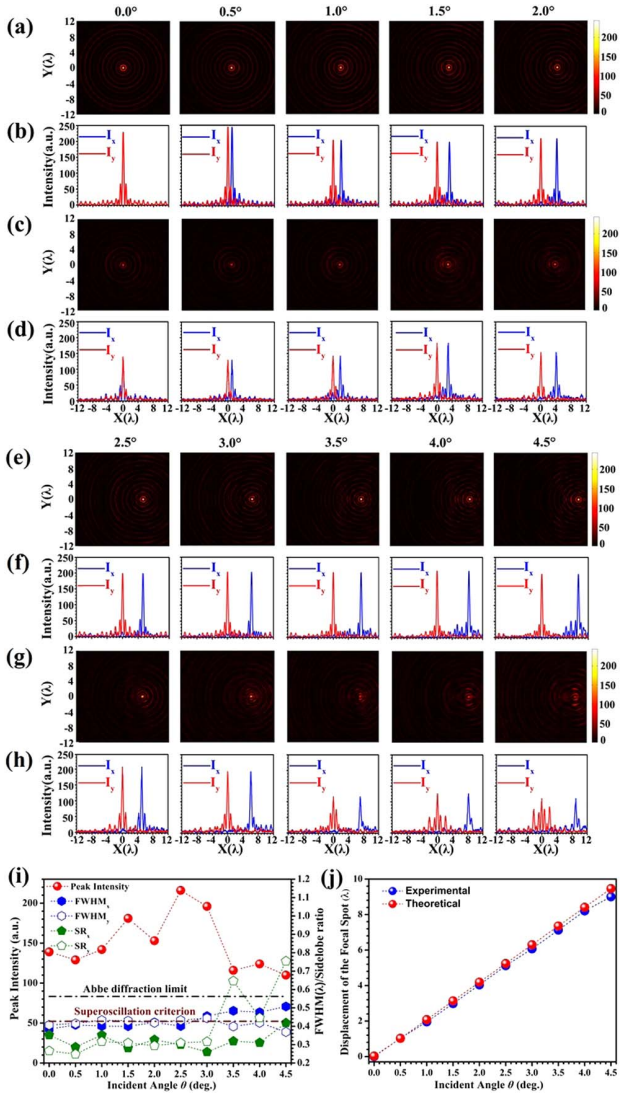

Fig. 4. Focusing performance of the flat-field superoscillation metalens. (a), (e) Simulation results of the optical intensity profile on the designed focal plane for different incident angles of 0°, 0.5°, 1.0°, 1.5°, 2.0°, 2.5°, 3.0°, 3.5°, 4.0°, and 4.5°; (b), (f) intensity distribution curves in x direction (blue) and y direction (red), both crossing the focal spot center; (c), (g) experimental results of the optical intensity profile on the designed focal plane for the 10 incident angles; (d), (h) intensity distribution curves in x direction (blue) and y direction (red), both crossing the focal spot center; (i) focusing performance parameters obtained from the experimental results, including peak intensity (red), spot size (FWHM) in x (blue solid) and y (blue open) directions and sidelobe ratio in x (green solid) and y (green open) directions; (j) spot displacement on the focal plane for the simulation result (red) and experimental result (blue).

xy plane were recorded through the digital camera at different z by scanning the one-dimensional nanopositioner.

The focal spots of the flat-field superoscillation metalens were measured with linearly polarized incident light and are shown along with simulation results in Figs. 4(a)–4(h) for different incident angles of 0°, 0.5°, 1.0°, 1.5°, 2.0°, 2.5°, 3.0°, 3.5°, 4.0°, and 4.5°. The incident plane is the xz plane. Figures 4(a) and 4(e) present the optical intensity distribution, and Figs. 4(b) and 4(f) give the intensity curves in x and y directions on the designed focal plane, while Figs. 4(c), 4(d), 4(g), and 4(h) display the experimental results, which show good agreement with theoretical predictions, especially when the incident angle is smaller than 3.5°. In the sidelobe, there is a clear increase at incident angles greater than 3.5°. The focusing performance parameters are presented in Fig. 4(i). It shows that for all tested incident angles, the spot sizes (full width at half maximum) in both x and y directions vary between 0.37λ and 0.507λ, which are smaller than the Abbe diffraction limit (0.562λ, 0.5λ/NA), as indicated by the black dashed line. However, compared with results obtained by simulations, there is a small increase in focal spot size. The sidelobe ratio is found to be smaller than 36% at a small incident angle, while it reaches 76% at the incident angle of 4.5°, which is also larger than numerical predictions. Figure 4(j) plots the focal spot displacement against the incident angle on the focal plane, where both numerical and experimental results are presented for comparison. Both results show good linear displacement with the incident angle. Although there is a small difference, the experimental results are consistent with the theoretical prediction. A displacement of approximately 9λ is achieved. Compared with a previously reported super-resolution singlet metalens, the field of view and the displacement have been enhanced by a factor of two. The discrepancy between the experimental and theoretical results may partially result from the assumption of uniform distribution of the optical fields within each meta-atom on the metalens surface during the diffraction pattern calculation, while the misalignment between the aperture stop and focusing lens can also contribute to this deviation.

Figure 5 presents the numerical and experimental results of intensity distribution and major focusing parameters, including peak intensity, spot size, and sidelobe ratio, on the xz plane at different incident angles, where the vertical dashed lines denote the position of the focal plane, and the Abbe diffraction limit of 0.562λ (0.5λ/NA) and superoscillation criterion of 0.427λ (0.38λ/NA) are given by the dashed curve and the dashed-dotted curve, respectively. Figures 5(a) and 5(e) illustrate the transversely polarized optical field intensity on the propagation plane obtained by the angular spectrum method; Figs. 5(b) and 5(f) plot the focusing parameters along the optical axis; Figs. 5(c) and 5(g) depict the transversely polarized optical field intensity on the propagation plane obtained in experiments; and Figs. 5(d) and 5(h) present the experimental focusing parameters along the optical axis. It is found that, different from previously report flat-field super-resolution metalenses [40,41], the flat-field superoscillation lens generates a unique needle-shaped non-diffraction beam with a propagation distance of 20λ at all tested incident angles. According to the simulation, in many parts of the needle, the transverse size is superoscillation. It is also interesting to find that all the needles are shifted in a way that they are parallel to each other at different incident angles. It seems that the lens can be treated as a superposition of series of local super-resolution axicons, or super-resolution Bessel beam generators. As pointed out above, the experimental results show a clear broadening in the transverse size of the needles, especially at larger incident angles.

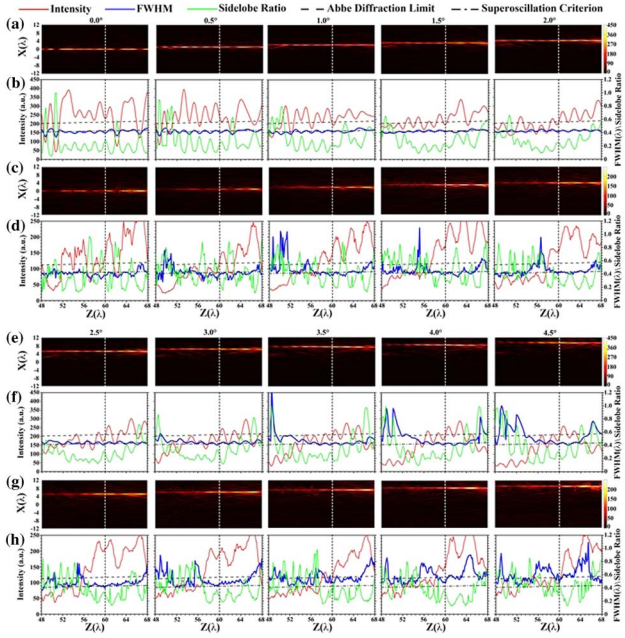

Fig. 5. Optical propagation properties on the incident plane (*xz* plane) at different incident angles. Simulation results: (a), (e) intensity distribution on *xz* propagation plane; (b), (f) peak intensity (red), FWHM (blue), and sidelobe ratio (green) along the propagation direction. Experimental results: (c), (g) intensity distribution on the *xz* propagation plane; (d), (h) peak intensity (red), FWHM (blue), and sidelobe ratio (green) along the propagation direction. The Abbe diffraction limit and superoscillation criterion are displayed by the dashed curve and dashed-dotted curve, respectively. The focal plane is denoted by the vertical dashed line.

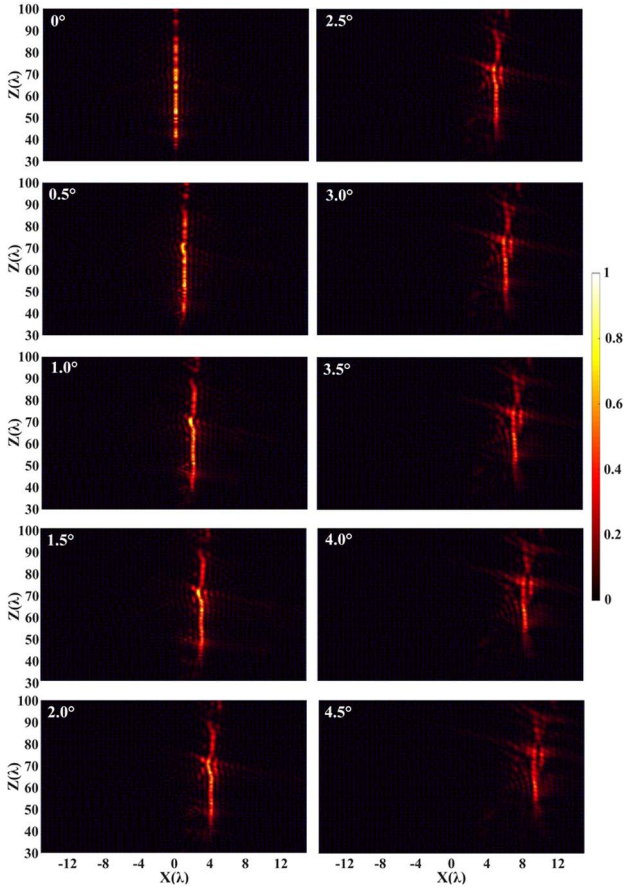

Fig. 6. Poynting vector on the incident plane (*xz* plane) at different incident angles, where the blue arrows give the direction of energy flow.

Figure 6 presents the Poynting vector on the incident plane (*xz* plane) between $z = 30\lambda$ and 100λ at different incident angles of 0°, 0.5°, 1.0°, 1.5°, 2.0°, 2.5°, 3.0°, 3.5°, 4.0°, and 4.5°, where the blue arrows give the direction of energy flow, and the strength of the energy flow is normalized. In all cases, there is a clear comparatively strong energy flow propagating along z direction. The length of the strong energy flow changes approximately from 45λ to 25λ as the incident angle increases from 0° to 4.5°. It is also noted that there is a deviation from the straight line in energy flow at $z = 70\lambda$, especially when the incident angle is greater than 2.0°. However, the energy flow remains almost in a straight line in the nearby region at the designed focal point of $z = 60\lambda$. This again indicates the unique property of the flat-field superoscillation lens. In our design, we made requirements only on the focusing parameters on the target focal plane without any restriction on energy flow in the propagation direction. According to our experience, the better the off-axis aberration is corrected, the smoother the generated focused field along the propagation direction will be. Therefore, we believe that such deviation can be further reduced when adopting a doublet metalens configuration, which can provide more freedom in the design to correct the off-axis aberration.

In the present design, the focusing efficiency is only approximately 1%. The low efficiency is due to three reasons. First, when the spot size decreases beyond the diffraction limit, the focusing efficiency usually drops sharply as the spot size decreases, especially when the spot size gets into the superoscillation regime. Second, there is only one functional phase surface in the present lens; the comparative large field of view is realized majorly by the aperture stop, which greatly limits the put-through of the entire incident light. Finally, the design of flat-field super-oscillatory lens is time communing, which makes it difficult to find the best optimal result in the design. The low efficiency may place a restriction on many practical applications. However, in certain cases, where the increase in resolution is priority, the low efficiency is not a big obstacle, such as in super-resolution microscopy demonstrated in label-free super-resolution microscopy based on super-resolution lenses [14,15].

5. CONCLUSION

In conclusion, we have demonstrated a dielectric metalens consisting of a-Si cubic geometric-phase meta-atoms and an optical aperture stop integrated on two sides of a 175-μm-thick SiO_2 substrate at wavelength $\lambda = 632.8$ nm, with a high NA of 0.89, focal length of 38 μm (60λ), radius of 152 μm (240λ), and field of view of 9°. The metalens with an optical aperture stop can effectively reduce the off-axis aberration, which not only allows it to work in the superoscillation regime but also greatly increases the field of view. Due to the availability of

substrate thickness, the distance between the optical aperture stop and the focusing lens is not optimized. Including this optimization in the design may further significantly improve the superoscillation focusing performance and field of view. In the present design, the designed spot size (smaller than 0.42λ) has already been in the superoscillation regime (smaller than $0.38\lambda/\mathrm{NA} = 0.427\lambda$), which leads to comparatively low focusing efficiency and also comparatively low signal-to-noise-ratio in the experiments. The co-axis alignment of the optical stop and the focusing metalens is challenging in fabrication, which will significantly influence the actual performance of the high-NA flat-field superoscillation metalens, especially when all parameters, including focal length, radius of the aperture stop, radius of the focusing lens, and substrate thickness, are comparatively small. This problem may become ignorable for a lens with a large size. Our work presents a promising theoretical and experimental proof of achieving a high-NA flat-field superoscillation metalens with large field of view, which can be further improved by achieving a flat-field super-resolution doublet metalens, or even multiple metalenses. Such a superoscillation metalens might offer a promising way toward superoscillation imaging and fast-scanning label-free far-field superoscillation microscopy.

Funding. National Natural Science Foundation of China (61927818); Natural Science Foundation of Chongqing (cstc2019jcyj-msxmX0315).

Acknowledgment. The authors extend sincere thanks to Prof. Ting Jiang and Prof. Yuanpeng Zou at the School of Foreign Languages and Cultures, Chongqing University, for their assistance in language polishing.

Disclosures. The authors declare no conflicts of interest.

Data Availability. The data that support the findings of this study are not publicly available at this time but may be obtained from the authors upon reasonable request.

[†]These authors contributed equally to this work.

REFERENCES

1. M. J. Rust, M. Bates, and X. Zhuang, "Sub-diffraction-limit imaging by stochastic optical reconstruction microscopy (STORM)," Nat. Methods **3**, 793–796 (2006).
2. E. Betzig, G. H. Patterson, R. Sougrat, O. W. Lindwasser, S. Olenych, J. S. Bonifacino, M. W. Davidson, J. L. Schwartz, and H. F. Hess, "Imaging intracellular fluorescent proteins at nanometer resolution," Science **313**, 1642–1645 (2006).
3. S. T. Hess, T. P. K. Girirajan, and M. D. Mason, "Ultra-high resolution imaging by fluorescence photoactivation localization microscopy," Biophys. J. **91**, 4258–4572 (2006).
4. F. Wei and Z. Liu, "Plasmonic structured illumination microscopy," Nano Lett. **10**, 2531–2536 (2010).
5. X. Liu, C. Kuang, X. Hao, C. Pang, P. Xu, H. Li, Y. Liu, C. Yu, Y. Xu, D. Nan, W. Shen, Y. Fang, L. He, X. Liu, and Q. Yang, "Fluorescent nanowire ring illumination for wide-field far-field subdiffraction imaging," Phys. Rev. Lett. **118**, 076101 (2017).
6. M. G. L. Gustafsson, "Nonlinear structured-illumination microscopy: wide-field fluorescence imaging with theoretically unlimited resolution," Proc. Natl. Acad. Sci. USA **102**, 13081–13086 (2005).
7. E. Abbe, "Beiträge zur Theorie des Mikroskops und der mikroskopischen Wahrnehmung," Archiv für Mikroskopische Anatomie **9**, 413–468 (1873).
8. M. V. Berry, "Evanescent and real waves in quantum billiards and Gaussian beams," J. Phys. A **27**, L391–L398 (1994).
9. M. V. Berry and S. Popescu, "Evolution of quantum superoscillations and optical superresolution without evanescent waves," J. Phys. A **39**, 6965–6977 (2006).
10. M. Berry, N. Zheludev, Y. Aharonov, F. Colombo, I. Sabadini, D. C. Struppa, J. Tollaksen, E. T. F. Rogers, F. Qin, M. Hong, X. Luo, R. Remez, A. Arie, J. B. Götte, M. R. Dennis, A. M. Wong, G. V. Eleftheriades, Y. Eliezer, A. Bahabad, G. Chen, Z. Wen, G. Liang, C. Hao, C. Qiu, A. Kempf, E. Katzav, and M. Schwartz, "Roadmap on superoscillations," J. Opt. **21**, 053002 (2019).
11. G. Chen, Z. Wen, and C. Qiu, "Superoscillation: from physics to optical applications," Light Sci. Appl. **8**, 56 (2019).
12. F. M. Huang and N. I. Zheludev, "Super-resolution without evanescent waves," Nano Lett. **9**, 1249–1254 (2009).
13. K. Huang, H. Ye, J. Teng, S. P. Yeo, B. Luk'yanchuk, and C. W. Qiu, "Optimization-free superoscillatory lens using phase and amplitude masks," Laser Photon. Rev. **8**, 152–157 (2014).
14. E. T. F. Rogers, J. Lindberg, T. Roy, S. Savo, J. E. Chad, M. R. Dennis, and N. I. Zheludev, "A super-oscillatory lens optical microscope for subwavelength imaging," Nat. Mater. **11**, 432–435 (2012).
15. F. Qin, K. Huang, J. F. Wu, J. H. Teng, C. W. Qiu, and M. H. Hong, "A supercritical lens optical label-free microscopy: sub-diffraction resolution and ultra-long working distance," Adv. Mater. **29**, 1602721 (2017).
16. G. Chen, K. Zhang, A. Yu, X. Wang, Z. Zhang, Y. Li, Z. Wen, L. Chen, L. Dai, S. Jiang, and F. Lin, "Far-field sub-diffraction focusing lens based on binary amplitude-phase mask for linearly polarized light," Opt. Express **24**, 11002–11008 (2016).
17. G. Chen, Y. Li, X. Wang, Z. Wen, F. Lin, L. Dai, L. Chen, Y. He, and S. Liu, "Super-oscillation far-field focusing lens based on ultra-thin width-varied metallic slit array," IEEE Photon. Technol. Lett. **28**, 335–338 (2016).
18. G. Chen, Y. Li, A. Yu, Z. Wen, L. Dai, L. Chen, Z. Zhang, S. Jiang, K. Zhang, X. Wang, and F. Lin, "Super-oscillatory focusing of circularly polarized light by ultra-long focal length planar lens based on binary amplitude-phase modulation," Sci. Rep. **6**, 29068 (2016).
19. G. Yuan, K. Rogers, E. T. F. Rogers, and N. I. Zheludev, "Far-field superoscillatory metamaterial superlens," Phys. Rev. Appl. **11**, 064016 (2019).
20. Y. W. Hu, S. W. Wang, J. H. Jia, S. H. Fu, H. Yin, Z. Li, and Z. Q. Chen, "Optical superoscillatory waves without side lobes along a symmetric cut," Adv. Photon. **3**, 045002 (2021).
21. E. T. F. Rogers, S. Savo, J. Lindberg, T. Roy, M. R. Dennis, and N. I. Zheludev, "Super-oscillatory optical needle," Appl. Phys. Lett. **102**, 031108 (2013).
22. G. Yuan, E. T. F. Rogers, T. Roy, G. Adamo, Z. Shen, and N. I. Zheludev, "Planar super-oscillatory lens for sub-diffraction optical needles at violet wavelengths," Sci. Rep. **4**, 6333 (2014).
23. A. P. Yu, G. Chen, Z. H. Zhang, Z. Q. Wen, L. R. Dai, K. Zhang, S. L. Jiang, Z. X. Wu, Y. Y. Li, C. T. Wang, and X. G. Luo, "Creation of sub-diffraction longitudinally polarized spot by focusing radially polarized light with binary phase lens," Sci. Rep. **6**, 38859 (2016).
24. G. Chen, Z. Wu, A. Yu, Z. Zhang, Z. Wen, K. Zhang, L. Dai, S. Jiang, Y. Li, L. Chen, C. Wang, and X. Luo, "Generation of a sub-diffraction hollow ring by shaping an azimuthally polarized wave," Sci. Rep. **6**, 37776 (2016).
25. Z. Wu, Q. Jin, K. Zhang, Z. Zhang, G. Liang, Z. Wen, A. Yu, and G. Chen, "Binary-amplitude modulation based super-oscillatory focusing planar lens for azimuthally polarized wave," Opto-Electron. Eng. **45**, 170660 (2018).
26. S. Zhang, H. Chen, Z. Wu, K. Zhang, Y. Li, G. Chen, Z. Zhang, Z. Wen, L. Dai, and L. Wang, "Synthesis of sub-diffraction quasi-non-diffracting beams by angular spectrum compression," Opt. Express **25**, 27104–27118 (2017).
27. Z. Wu, K. Zhang, S. Zhang, Q. Jin, Z. Wen, L. Wang, L. Dai, Z. Zhang, H. Chen, G. Liang, Y. Liu, and G. Chen, "Optimization-free approach for generating sub-diffraction quasi-non-diffracting beams," Opt. Express **26**, 16585–16599 (2018).

28. Z. Wu, Q. Jin, S. Zhang, K. Zhang, L. Wang, L. Dai, Z. Zhang, Z. Wen, G. Liang, Y. Liu, and G. Chen, "Generating a three-dimensional hollow spot with sub-diffraction transverse size by a focused cylindrical vector wave," Opt. Express **26**, 7866–7875 (2018).
29. R. Zuo, W. Liu, H. Cheng, S. Chen, and J. Tian, "Breaking the diffraction limit with radially polarized light based on dielectric metalenses," Adv. Opt. Mater. **6**, 1800795 (2018).
30. Q. He, S. Sun, S. Xiao, and L. Zhou, "High-efficiency metasurfaces: principles, realizations, and applications," Adv. Opt. Mater. **6**, 1800415 (2018).
31. S. Chen, Y. Zhang, Z. Li, H. Cheng, and J. Tian, "Empowered layer effects and prominent properties in few-layer metasurfaces," Adv. Opt. Mater. **7**, 1801477 (2019).
32. Y. B. Zhang, H. Liu, H. Cheng, J. G. Tian, and S. Q. Chen, "Multidimensional manipulation of wave fields based on artificial microstructures," Opto-Electron Adv. **3**, 200002 (2020).
33. X. G. Luo, "Subwavelength optical engineering with metasurface waves," Adv. Opt. Mater. **6**, 1701201 (2018).
34. Q. Fan, W. Xu, X. Hu, W. Zhu, T. Yue, C. Zhang, F. Yan, L. Chen, H. J. Lezec, Y. Lu, A. Agrawal, and T. Xu, "Trilobite-inspired neural nanophotonic light-field camera with extreme depth-of-field," Nat. Commun. **13**, 2130 (2022).
35. Y. Hu, X. Wang, X. Luo, X. Ou, L. Li, Y. Chen, P. Yang, S. Wang, and H. Duan, "All-dielectric metasurfaces for polarization manipulation: principles and emerging applications," Nanophotonics **9**, 3755–3780 (2020).
36. Y. Wang, Q. Fan, and T. Xu, "Design of high efficiency achromatic metalens with large operation bandwidth using bilayer architecture," Opto-Electron. Adv. **4**, 200008 (2021).
37. A. Kalvach and Z. Szabó, "Aberration-free flat lens design for a wide range of incident angles," J. Opt. Soc. Am. B **33**, A66–A71 (2016).
38. B. Groever, W. T. Chen, and F. Capasso, "Meta-lens doublet in the visible region," Nano Lett. **17**, 4902–4907 (2017).
39. A. Arbabi, E. Arbabi, S. M. Kamali, Y. Horie, S. Han, and A. Faraon, "Miniature optical planar camera based on a wide-angle metasurface doublet corrected for monochromatic aberrations," Nat. Commun. **7**, 13682 (2016).
40. M. B. Pu, X. Li, Y. H. Guo, X. L. Ma, and X. G. Luo, "Nanoapertures with ordered rotations: symmetry transformation and wide-angle flat lensing," Opt. Express **25**, 31471–31477 (2017).
41. Q. Zhang, F. Dong, H. Li, Z. Wang, G. Liang, Z. Zhang, Z. Wen, G. Chen, L. Dai, and W. Chu, "High-numerical-aperture dielectric metalens for super-resolution focusing of oblique incident light," Adv. Opt. Mater. **8**, 1901885 (2020).
42. Z. Li, C. Wang, Y. Wang, X. Lu, Y. Guo, X. Li, X. Ma, M. Pu, and X. G. Luo, "Super-oscillatory metasurface doublet for sub-diffraction focusing with a large incident angle," Opt. Express **29**, 9991–9999 (2021).
43. S. Pancharatnam, "Generalized theory of interference and its applications," Proc. Indian Acad. Sci. Sect. A **44**, 398–417 (1956).
44. M. V. Berry, "The adiabatic phase and Pancharatnam's phase for polarized light," J. Mod. Opt. **34**, 1401–1407 (1987).
45. N. Jin and Y. Rahmat-Samii, "Advances in particle swarm optimiza tion for antenna designs: real-number, binary, single-objective and multiobjective implementations," IEEE Trans. Anntenas Propag. **55**, 556–567 (2007).
46. L. Novotny and B. Hecht, *Principles of Nano-Optics* (Cambridge University, 2006).